Journal of Power Sources 466 (2020) 228305

Contents lists available at ScienceDirect

Journal of Power Sources

journal homepage: www.elsevier.com/locate/jpowsour

Photosynthesis of H_2 and its storage on the Bandgap Engineered Mesoporous (Ni^{2+}/Ni^{3+})O @ TiO_2 heterostructure

Kumar Raju [a], Saravanan Rajendran [b,*], Tuan K.A. Hoang [c], D. Durgalakshmi [d], Jiaqian Qin [e], D. E. Diaz-Droguett [f], F. Gracia [g], M.A. Gracia-Pinilla [h,i]

[a] Energy Centre, Council for Scientific and Industrial Research (CSIR), Pretoria, 0001, South Africa
[b] Faculty of Engineering, Department of Mechanical Engineering, University of Tarapacá, Avda, General Velasquez, 1775, Arica, Chile
[c] Centre of Excellence in Transportation Electrification and Energy Storage, Hydro-Québec, 1806, boul Lionel-Boulet, Varennes, J3X 1S1, Canada
[d] Department of Medical Physics, Anna University, Chennai, 600025, India
[e] Research Unit of Advanced Materials for Energy Storage, Metallurgy and Materials Science Research Institute, Chulalongkorn University, Bangkok 10330, Thailand
[f] Institute of Physics, Facultad de Física, Pontificia Universidad Catolica de Chile, Casilla 306, Santiago, Chile
[g] Department of Chemical Engineering, Biotechnology and Materials, University of Chile, Beauchef 851, 6th Floor, Santiago, Chile
[h] Universidad Autónoma de Nuevo León, Facultad de Ciencias Físico-Matemáticas, Av. Universidad, Cd. Universitaria, San Nicolás de los Garza, NL, Mexico
[i] Universidad Autónoma de Nuevo León, Centro de Investigación en Innovación y Desarrollo en Ingeniería y Tecnología, PIIT, Apodaca, N.L, Mexico

HIGHLIGHTS

- Mesoporous (Ni^{2+}/Ni^{3+})O @ TiO_2 is simply synthesized with targeted bandgap & defects.
- For H_2 storage, about 480% enhancement is achieved via Kubas interaction mechanism.
- For H_2 photosynthesis, 1200% improvement is achieved due to higher efficiency.

ARTICLE INFO

Keywords:
Hydrogen
Adsorption
Photocatalyst
Nanomaterial
Surface defect

ABSTRACT

A noble-metal free and surface defect-induced mesoporous mixed valent NiO decorated TiO_2 heterostructure with tuned bandgap has been successfully prepared. Its outstanding visible-light driven hydrogen evolution and its excellent H_2 storage ability have been examined and confirmed. The formation of oxygen vacancies by surface defect creates the Ni^{3+} and Ti^{3+} on the interface of the heterostructure induce the efficient H_2 evolution, benchmarked by 1200% enhancement in catalytic performance. The underlying chemistries include the near-unity occupancy of e_g orbital (t_{2g}^6 e_g^1) of Ni^{3+} which speeds up the electron transfer and significantly promote the excellent electron-hole separation efficiency, establishes the outstanding overall charge-transfer efficiency and long-term photocatalytic activity in the visible light spectrum. Multiple Ti^{3+} adsorption centers in the structure attract multiple intact H_2 molecules per each center via a sigma - pi bonding motif - namely the Kubas interaction - which leads to 480% higher H_2 adsorption capability against the performance of the pristine mesoporous TiO_2. Not only the significant results, the study also provide an air-stable synthetic method on the basis of low-cost and abundant materials, which are strongly favoured for scaling up production.

1. Introduction

Motivated by the abundance of solar energy and contains *ca.* ~46% visible light than that of UV-light (~4%) in the solar spectrum, the development of low bandgap materials for visible-light-driven hydrogen generation is pioneered [1,2]. The eco-friendly TiO_2 semiconductor photocatalyst has attracted extensive interests over the past decade as a benchmark material for photocatalytic splitting the water into hydrogen and oxygen under UV-light irradiation to generate hydrogen as the clean and renewable fuel [3–5]. Although an adequate photocatalytic activity acquired under UV-light, the rapid recombination of electrons and holes potentially limits the high performance [6,7]. To alleviate this critical challenge, engineering the bandgap of TiO_2 which inherits exotic electronic and optical properties is a viable step to apart electrons and holes

* Corresponding author.
E-mail address: saravanan3.raj@gmail.com (S. Rajendran).

https://doi.org/10.1016/j.jpowsour.2020.228305
Received 27 October 2019; Received in revised form 28 April 2020; Accepted 2 May 2020
Available online 20 May 2020

for minimizing their re-combination [8–11]. In this regard, several strategies have been proposed for engineering the band gap of TiO_2 (~3.2 eV) to expand the absorption capability into visible light range ($\lambda > 420$ nm) [1,12,13]. The fine-tuning of TiO_2 band gap by possible modification methods including metal and non-metal doping, the selective exposure of reactive crystallographic facets, noble metal deposition, and the formation of heterojunction with n- and p-type transition metal oxides. For instant, TiO_2/CuO [14,15] NiO/TiO_2 [11,16–18], and CoO/TiO_2 [19] have been widely investigated [20–22]. Despite noble metals (Pt, Au, and Pd) deposited on TiO_2 exhibited high photocatalytic H_2 production ability, the high costs of the noble metals impede their practical application at the large scale. Furthermore, the group-VIII metals are easily poisoned by impurities [23–28]. As a consequence, enormous effort has been devoted to engineer the TiO_2 band gap by introducing the p-n heterojunction using other transition metal oxides, e.g. CuO, NiO, ZnO, Cu_2O [14,29–31] Amongst, NiO, a wide bandgap of ~3.5 eV p-type semiconductor with possessing rapid h^+ mobility and high charge carrier concentration is a promising candidate for the fabrication of the p-n heterojunction with mesoporous TiO_2 [29,32].

NiO has been reported as co-catalyst in TiO_2 for active H_2 photosynthesis using visible light sources, associated with a significantly higher enhancement in charge carrier lifespan comparing with that of metallic Ni and $Ni(OH)_2$ materials [11,33,34]. Motivated by the design principle of Yang et al. [35] and the formation of the heterojunction between *p*- and *n*-type semiconductor transition metal oxides, we explore the potential strategy to create surface defects on the composite which will induce the formation of nickel vacancies and to enable the space-charge region at the interface between the *p*-type and *n*-type of heterojunction, thereby promoting the H_2 production [36,37]. Therefore, we have synthesized defect induced mesoporous mixed-valent NiO @ TiO_2 nanocomposite consisting an adequate amount of Ni^{3+} by combining a sol-gel method and thermal decomposition to synthesize the targeted material. The construction of surface defects on the composite significantly altered the electronic configuration of Ni^{2+}, and creating Ni^{3+} comprising the electronic configuration of t_{2g}^6 e_g^1, expressing surface cation e_g orbital occupancy of about unity and high covalent metal-oxygen bonding facilitates the sustainable photocatalytic activity [38]. Besides, the formation of heterojunction promoting Ti^{3+} and Ni^{2+} active sites associated with an intimate interface and Ni^{3+} from surface defects leads to the diminishing of the fast recombination of photoinduced electrons and holes. Thus, the reasonably impressive separation efficiency of photoexcited electron-hole pairs is achieved. This endows a 12-fold enhancement of catalytic performance.

The hydrogen adsorption ability of Ti^{3+} containing materials has been widely investigated in the literature [39]. Most of which were related with intensive organometallic synthesis [40–42]. To the best of our knowledge, the interaction of Ti^{3+} which were generated via p-n heterojunction formation with dihydrogen molecules is not well studied. Thus, we were motivated to elaborate the hydrogen storage properties of such Ti^{3+} containing species. It is even more meaningful that the synthesis of such materials is simple and do not require stringent organometallic synthesis. To our surprise, the synthetic material exhibits nearly 500% enhancement of hydrogen sorption capacity in the very low pressure region.

2. Experimental procedure

2.1. Preparation of mesoporous TiO_2 and mixed-valent NiO@TiO_2

The detailed experimental procedure and physicochemical characterization techniques used are well described in our recent report [43]. Typically, the mesoporous TiO_2 nanoparticles was prepared by dissolving 30 ml of titanium tetra-isobutoxide in 150 ml of isopropyl alcohol (1:5 ratio) under continuous stirring at 600 rpm followed by the drop-wise addition of 0.5 M citric acid into the colloidal mixture to form gel. The resulted white gel was then dried at 150 °C for 30 min and the pre-synthesized white powder subjected to calcination at 450 °C for 1 h to yield mesoporous TiO_2 nanoparticles.

The preparation of mixed-valent mesoporous NiO@TiO_2 nanocomposites has been reported in our recent publication [43]. In a typical experiment, as-prepared mesoporous TiO_2 powder and nickel acetate (9:1) was grounded and then calcined at 450 °C for 3h. After the vaporization of water and acetate from the decomposed metal acetate precursors, the condensation reaction permits the nucleus to grow on the surface of the mesoporous TiO_2 by the slow cooling process to deliver the mixed-valent NiO@TiO_2 nanocomposite. The X-ray fluorescence (XRF) analysis was used to quantify the ratio of TiO_2 and NiO, and it is found to be 95.5:4.5 in the product.

2.2. Material characterization

Powder X-ray diffaction (D5000 diffractometer, Siemens, USA with $CuK_{\alpha 1}$ radiation ($\lambda = 1.5406$ Å)) was used to verify the crystal structures of the obtained mesoporous TiO_2 and NiO@TiO_2 nanocomposite samples. The high-resolution transmission electron microscopy (HRTEM) and elemental mapping of as-prepared samples were carried out on FEI TITAN G2 80-300 operating at 300 kV. X-ray fluorescence (XRF, EDX-720, Shimadzu) was used to characterize the chemical composition. The oxidation states and surface elements of the samples were revealed by X-ray photoelectron spectroscopy (XPS), using a Thermo Scientific Escalab 250Xi. The nitrogen adsorption-desorption processes were performed on a Micromeritics ASAP 2020 (USA), through which we obtained the total surface area and pore distribution properties. Raman measurements were attained from Jobin-Yvon micro Raman spectrometer with 532 nm line of an argon ion laser as the exciting light source with 4 mW power. The UV–Vis diffuse reflectance spectra (VARIAN CARY 5E, USA) were recorded at room temperature by UV-VIS-NIR Spectrophotometer.

2.3. Photosynthesis of hydrogen gas

In a typical photocatalytic water splitting reaction, 100 mg of as-obtained mesoporous NiO@TiO_2 catalyst was dispersed in 200 ml of methanol-water (1:1) mixture in a 250 ml photoreactor, which was maintained with constant temperature near ambient (25 °C). Before the hydrogen generation experiment, argon was bubbled for 20 min to remove the dissolved oxygen. The photocatalytically generated H_2 was periodically monitored using a PerkinElmer Autosystem gas chromatography equipped with a flame ionization detector (FID) and a thermal conductivity detector (TCD).

2.4. Hydrogen storage characterization

A quartz-crystal microbalance (QCM) method on MDC model SQM-310 was used for elucidating the hydrogen storage capacity of the synthetic materials. The experimental procedure was reported in our recent report [44]. In a standard experiment, a sample (TiO_2 or NiO@TiO_2) were sonicated in isopropanol alcohol for 5 min followed by casting the suspension onto the quartz crystal (QC) at room temperature. The QC was placed in the head of the QCM system and maintained the QC temperature around 20 °C in a vacuum chamber during the entire measurement process. An appropriate amount of H_2 (Indura, 99.995%, $O_2 < 5$ ppm, $H_2O < 8$ ppm, CO_2+CO < 4 ppm, $N_2 < 20$ ppm, and THC < 5 ppm) was injected into the chamber with different pressure intervals ranging from 3 to 100 Torr. The mass changes upon H_2 adsorption by the samples were determined by monitoring in-situ changes of resonance frequency (Δf) of QC for 7 min. The relationship between the gained mass (Δm) on the QC from H_2 adsorption and their resonance frequency shift (Δf) is quantified by the Sauerbrey's equation [45,46].

$$\Delta f = -\frac{2f_0^2}{A\sqrt{\rho \cdot \mu}}\Delta m \quad (1)$$

where, f_0 = Resonance frequency of the fundamental mode (Hz), Δf = Frequency change (Hz).

Δm = Mass change (g), A = effective area of the QC (cm^2), ρ = density of the QC (g/cm^3) and μ = Bulk modulus for QC.

The above equation provides the relationship between the negative variation of the QC resonance frequency and the mass gain of the prepared samples upon H_2 adsorption.

3. Results and discussion

The surface defect-induced mesoporous mixed-valent NiO (Ni^{2+}/Ni^{3+}) @ TiO_2 nanocomposite heterostructure was successfully synthesized by utilizing the combined synthesis strategy of the sol-gel route followed by thermal decomposition. The structure of synthetic materials was characterized by powder X-ray diffraction (XRD). Furthermore, the materials were studied by XPS, Raman, TEM, DRS, and thermal analysis. A detailed report of XRD and XPS data for this material can be found in our recent publication [43]. In brief, Fig. 1(a–d) describe the physical features of mesoporous TiO_2 and NiO @ TiO_2. The XRD patterns of pristine TiO_2 and defect-induced NiO @ TiO_2 was depicted as Fig. 1a, labeled with their corresponding hkl planes. The inset highlighted in Fig. 1a clearly indicates the peak originating from NiO at $2\theta = 43.18^\circ$ corresponding to 200 planes of cubic NiO (JCPDS No: 47-1049) without affecting the TiO_2 tetragonal phase.

Raman scattering was measured to examine the structural changes associated with peak position and their intensities in TiO_2 upon insertion of NiO and showed in Fig. 1b, the inset highlights the expansion of intensity. As expected, Raman active fundamentals obtained at 145.6, 198.7, 395.9, 516.2, and 637.7 cm^{-1} associated with Eg, Eg, B1g, A1g, B1g + A1g and Eg modes, respectively for NiO @ TiO_2 heterostructure nanocomposite, showing the significant reduction in intensity along with a slight shift in peak positions than those of pristine anatase TiO_2 corresponding to the Raman active shifts at 145.2, 197.3, 397.2, 516.9, and 639.7 cm^{-1}. The calculated FWHM of the intense sole Raman active at ~145 cm^{-1} (Eg) is to be 16.40 and 16.89 cm^{-1} for NiO @ TiO_2 and TiO_2, respectively. These results suggest the structural changes associated with peak broadening of NiO@TiO_2 and comparably small FWHM than pristine counterpart are attributed to the formation of oxygen vacancies, surface defects and/or the reduction of Ti^{4+} into Ti^{3+}, and the formation of Ni^{3+} in the lattice. The high-resolution XPS was used as a highly sensitive tool to examine the interactions between the chemical compositions and their chemical status of the prepared samples of TiO_2 and NiO incorporated TiO_2. Fig. 1c-e describe the deconvoluted spectra of O1s, Ti $2p_{3/2}$ (c and d) and Ni $2p_{3/2}$ (e) for both pristine TiO_2 and NiO @ TiO_2 composite, respectively. As expected, the presence of surface defects on the TiO_2 lattice by NiO addition, the formation of oxygen vacancies and electron attraction near the NiO @ TiO_2 heterojunction interface significantly alter the binding energy of Ti^{3+} and Ti^{4+} in Ti $2p_{3/2}$ spectra (Fig. 1d) of NiO @ TiO_2 at 456.35 and 456.88 eV than that of neat TiO_2 at 457.2 and 458.12 eV, respectively. Besides, the lowering the binding energy can also be attributed to the enhancement of electron density of Ti by partial electron sharing of electronegative oxygen of Ni to Ti, and the formation of Ni^{3+} by oxidation of surface Ni^{2+} at the heterojunction interface to attain the charge neutrality creates the Ti^{3+} near the interface. A substantial increment of Ti^{3+} (oxygen vacancies) concentration observed as result of intense peak in NiO @ TiO_2 leading to low binding energy witnessed at 456.35 eV, offering the improvement of electrical conductivity of heterostructure. The O 1s region (Fig. 1c) also displays the considerable chemical shift in binding energy at 529.30 eV (~529.48 eV for TiO_2) consists of integral split peaks at 530.90 and 531.51 eV corresponds to oxygen bonded with Ti^{4+}, Ni^{2+}, and Ni^{3+}, respectively. However, a small shift in oxygen bonding in the O 1s spectra after NiO addition clearly justifies the creation of Ti^{3+} in the lattice near the oxygen vacancies and Ni^{3+} near the Ni vacancies. Fig. 1 e shows the further evidence of the formation of Ni^{2+} and Ni^{3+} in the p-n

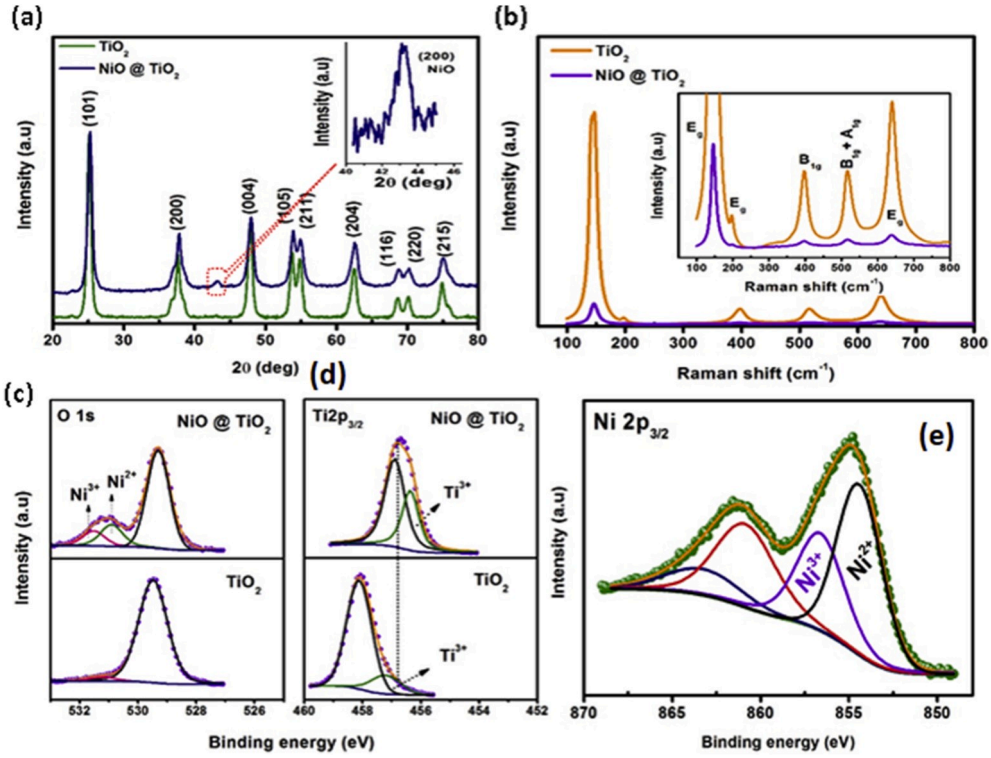

Fig. 1. Physical characterization of pristine TiO2 and NiO@TiO2. (a) XRD pattern of neat TiO2 and NiO@TiO2 with their corresponding lattice plane, inset shows the magnified view of (200) plane of NiO. (b) Raman scattering of pristine TiO2 and NiO@TiO2, inset shows the magnified view of the intensity with their symmetry representation. X-ray photoelectron spectroscopy (XPS) profiles of (c) O1s, (d) Ti 2p3/2 of pristine TiO2 and NiO @ TiO2, (e) Ni 2p3/2 of NiO @ TiO2 respectively.

heterostructure. The characteristic Ni $2p_{3/2}$ peak obtained at 854.93 eV, further deconvoluted to 854.52 and 856.75 eV are assigned to Ni^{2+} and Ni^{3+}, respectively, indicates about 30% of Ni^{3+} concentration present in the heterostructure composite. Thus, the XPS results clearly revealed that the NiO @ TiO_2 composite having a substantial amount of Ni^{3+} and Ti^{3+} at the heterojunction interface, expecting to impart high donor densities and high electrical conductivity which are essential for efficient catalysts.

As shown in Fig. 2(a–c), the TEM and HR-TEM observation confirm the formation of well-scattered porous network of NiO spherical particles on the TiO_2 surface with an average particle size of 8 nm which were homogenously decorated with larger TiO_2 particles (~18 nm in size). HAADF (Fig. 2b) further demonstrates the well-dispersion of NiO particles on the TiO_2 matrix. Fig. 2c shows the magnified view of the HR-TEM image of NiO @ TiO_2 which has more line dislocation or linear defect on the NiO and TiO_2 which are highlighted by the circle mark. Moreover, the high resolution TEM image (Fig. 2d) discloses the crystalline nature of particles comprising the clear lattice fringes with the interplanar distances of 0.35 nm, 0.237 nm and 0.28 nm corresponding to the lattice planes of (101), (004) and (200) perfectly matched to the tetragonal anatase TiO_2 and cubic NiO, respectively. Remarkably, the extended view of HR-TEM image (Fig. 2e) further evidences the heterostructure particles having both clear lattice fringes and fuzzy outer edges, implying the disordered phase on the particle surface. As illustrated in Fig. 2f, the ring pattern obtained for NiO @ TiO_2 from selected area electron diffraction (SAED) was well-indexed with their corresponding lattice planes belonging to the tetragonal TiO_2 and cubic NiO, respectively in agreement with the data obtained from XRD analysis. More evidently, an elemental mapping of NiO@TiO_2 obtained from energy dispersive X-ray (EDX) analysis and the detected constituents are displayed as Ti, Ni and O. Thus, the images clearly demonstrate the heterostructure containing well-dispersed particles of Ti and Ni in the composite.

An efficient utilization of visible light for H_2 evolution requires a narrow bandgap of semiconductors. However, to estimate the bandgap energy, diffusive reflectance spectroscopic (DRS) analysis was carried out for neat TiO_2 and NiO @ TiO_2 samples and the observed reflectance spectra are shown in Fig. 3a and b. A considerable red shift in the absorption edge towards visible region occurred after the inclusion of NiO into the TiO_2 crystal lattice and found to be about 450 nm when compared to TiO_2 (~380 nm). Besides, the estimated bandgap energy by Kubelka-Munk function against the energy of light is displayed in Fig. 3b, and found to be 3.27 eV and 2.82 eV for TiO_2 and NiO@TiO_2, respectively. Indeed, the formation of disorderliness and oxygen vacancies at the heterojunction leads to uplifting the valence band and lowering the conduction band, resulting in narrowing the bandgap energy [29]. As evidenced by our XPS and TEM analysis, the formation of Ti^{3+} and Ni^{3+} due to the oxygen vacancies and surface defects near the interface, and the line defects on the surface, suggesting that the narrow bandgap of NiO@TiO_2 could be attributed to both uplift of the valence band and lower the conduction band.

The high specific surface area comprising an adequate pore structure is a critical element for efficient photocatalyst. The N_2 adsorption-desorption analysis was carried out using BJH and BET methods. The resulted N_2 sorption isotherms and the corresponding pore diameter distribution for neat TiO_2 and NiO@TiO_2 are depicted in Fig. 3 c and d. It can be clearly seen from Fig. 3 c and d, that the appearance of the H3-type hysteresis loop for NiO @ TiO_2 enlightening the presence of

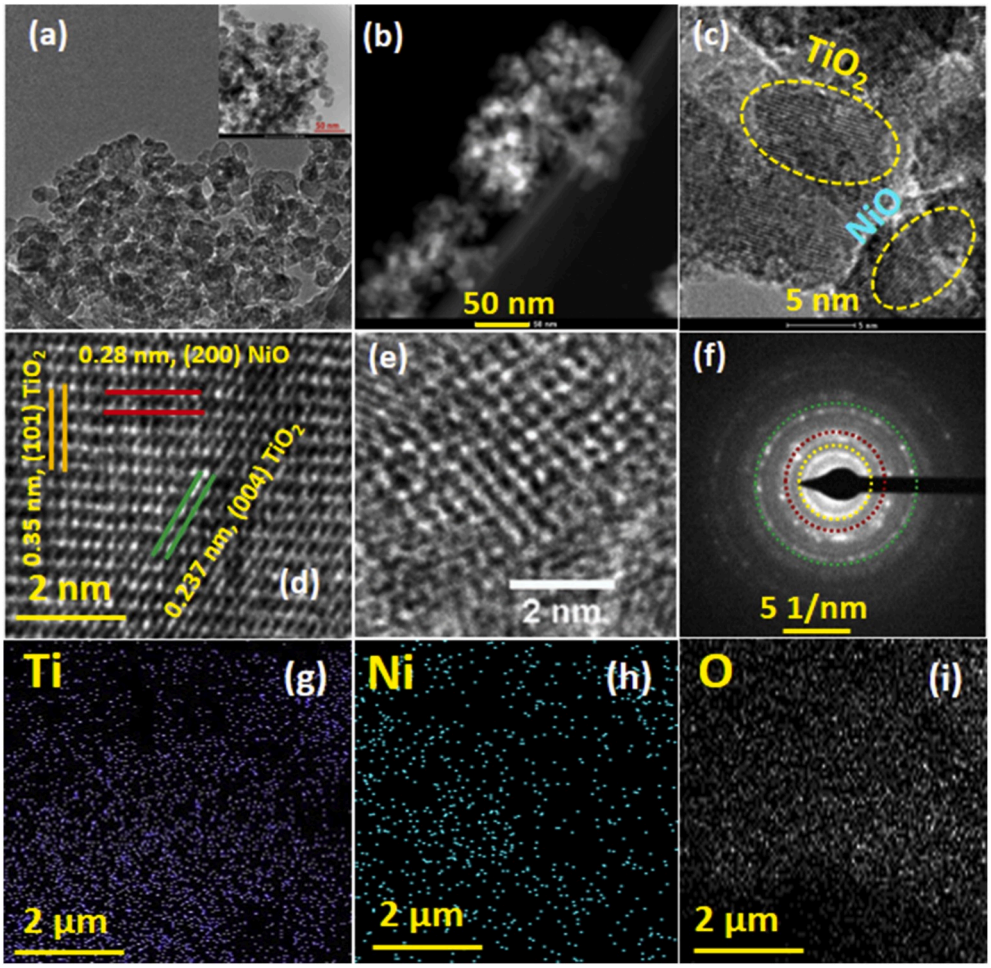

Fig. 2. Morphological analyses of NiO@TiO_2. (a) Transmission electron microscopy (TEM) image, inset shows the shake of clarity to view the dark and white parts of the NiO and TiO_2 particles infers the formation with well-defined distribution. (b) HAADF profile of NiO@TiO_2 also shows the dark and bright field. (c and d) HR-TEM image shows the clear inter-planner distance with their corresponding lattice planes, magnified view of the lattice fringes confirm the TiO_2 and NiO on the amorphous region (e and f) SAED pattern of the NiO@TiO_2 shows the ring pattern of lattice planes. (g, h and i) Elemental mapping images of Ti, Ni and O.

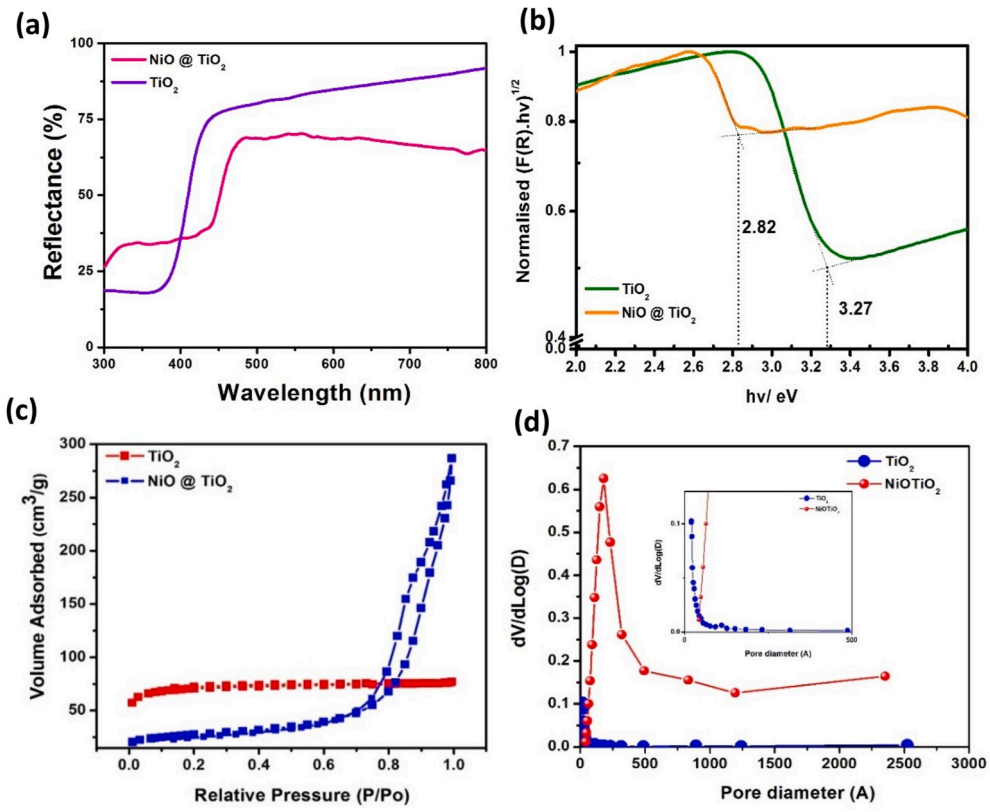

Fig. 3. **(a)** Diffusive reflectance spectroscopy (DRS) plots of neat TiO_2 and NiO @ TiO_2. (b) Bandgap energy estimated by Kubelka-Munk function against the energy of light. (c) N_2 –adsorption-desorption isotherms and the corresponding pore diameter distribution (d) for neat TiO_2 and NiO@TiO_2

mesopores on the surface with the diameter about ~15 nm, while the TiO_2 shows the H4-type hysteresis with the pore diameter about ~2 nm. A significant drop in BET surface area is obtained and found to be 94.26 m^2/g for NiO@TiO_2 heterostructure compared with that of TiO_2 (238.9 m^2/g). This may be due to the loss of mesoporosity with the pore diameter of about ~2 nm. We assume that the NiO addition may lead to the blocking some of original TiO_2 mesopores due to the deposition and subsequent decomposition of the Ni precursor during heat treatment. However, the introduction of NiO may lead to the connection of small TiO_2 nanoparticles to deliver larger pore area, as evidences the increase in pore volume was estimated to be 0.356 cm^3/g compared to pure TiO_2 (0.117 cm^3/g). This behaviour was observed previously on the Ag doped TiO_2 materials, which exhibits a gain in pore volume and the nitrogen sorption quantities at high relative pressure. In that case, it was related to the introduction of line defects in the Ag doped TiO_2 materials vs the pristine TiO_2 [44]. Despite having a low surface area, the NiO@TiO_2 remains mesoporous, and the surface defects consisting of Ti^{3+} and Ni^{3+} at the heterojunction interface elegantly improves the photoexcited electron-hole separation and transfer efficiency.

The photocatalytic performance of H_2 production from H_2O on the TiO_2 and NiO @ TiO_2 photocatalysts were evaluated under UV and visible-light irradiation using ethanol as a sacrificial agent. As shown in Fig. 4a, under visible-light irradiation, a very low H_2 production (37 μmol g^{-1}) is observed for neat TiO_2, whereas a significant increase in H_2 production found to be 430 μmol g^{-1} for NiO @ TiO_2. This is about 12 times higher than that of TiO_2. Under UV radiation, the NiO @ TiO_2 is still outperforming the pristine TiO_2. A linear increment of H_2 evolution is observed for NiO@TiO_2, estimated to be 1850 μmol g^{-1} which is 2 times higher than the amount of H_2 obtained from pristine TiO_2 (978 μmol g^{-1}) (Fig. 4b). Fig. 4c clearly describes the estimated amount of hydrogen production on the neat TiO_2 and NiO@TiO_2 photocatalysts under different irradiation condition. The obtained remarkable hydrogen production rate of about 1.87 mmol g^{-1} h^{-1} under visible-light for NiO@TiO_2 compared to that of the values reported in TiO_2/NiO/rGO (0.24 mmol h^{-1} g^{-1}) [32], NiO/TiO_2 (1.2 mmol h^{-1} g^{-1}) [11], and NiOQD/TiO_2 (1.35 mmol h^{-1} g^{-1}) [47] clearly infer its exceptional advantages of NiO@TiO_2 which can be explained as follows. The formation of significant concentrations of Ni^{3+} and Ti^{3+} by surface defects and oxygen vacancies are creating effective active sites and high electron density relatively contributing to the excellent electron-hole separation efficiency, resulting in the enhancement of overall charge-transfer efficiency. In addition, the creation of Ni^{3+} active sites by Ni^{2+} oxidation at the heterojunction interface establishes the near-unity occupancy of e_g orbital ($t_{2g}^6 e_g^1$) and this assists to speed up the electron transfer. Thus, the abundant interface formation near the interface on NiO@TiO_2 p-n heterojunction significantly promotes the active sites for rapid electron and ion transfer processes, establishing an efficient H_2 production under visible-light irradiation. Another excellent advantage of NiO@TiO_2 is its outstanding durability, which is highly desirable for long-term photocatalytic activity. The photocatalytic cycling was executed in four-run cycles (20 h) and each run lasted for 5 h, and the observed results are shown in Fig. 4d. It can be clearly seen that the NiO@TiO_2 is still retained its photocatalytic activity elegantly with no obvious loss upon three repeated cycles, signifying the long-lasting photocatalytic activity of NiO@TiO_2.

Fig. 5 (a and b) describes the H_2 adsorption isotherm of as-prepared mesoporous TiO_2 and NiO @ TiO_2 photocatalyst as a function of hydrogen exposure pressure. The co-existence of Ni^{3+} and Ti^{3+} together with Ni^{2+} and Ti^{4+} in NiO@TiO_2 heterostructure facilitates the multiple intact of H_2 molecule with Ti^{3+} via the σ-π bonding motif, in which H_2 donates its two electrons to Ti^{3+} to form the sigma bonding and the Ti^{3+} donates its filled d^1 electron back to the antibonding orbital σ* of the H_2 molecule. The antibonding orbital σ* is respected to hydrogen and considered as a bonding between Ti and H, which release the excess electron density of Ti upon accepting multiple H_2 molecules [48]. The heterostructure, NiO@TiO_2 adsorbs ~1.2 wt% of hydrogen at 100 Torr

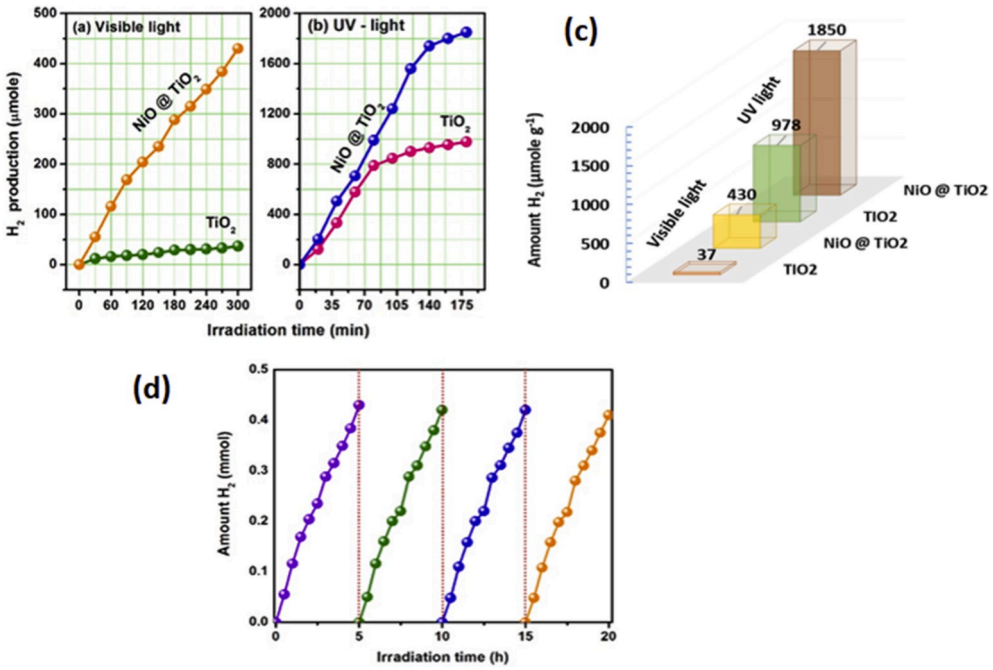

Fig. 4. The photocatalytic performance of H_2 evolution from H_2O on the TiO_2 and NiO @ TiO2 photocatalysts evaluated under (a) visible- and (b) UV -light irradiation. (c) The estimated amount of hydrogen production on the neat TiO_2 and NiO@TiO_2 photocatalysts under different light irradiation. (d) The photocatalytic cycling of NiO @ TiO_2 executed in four-run cycles (20 h) and each run lasted for 5 h.

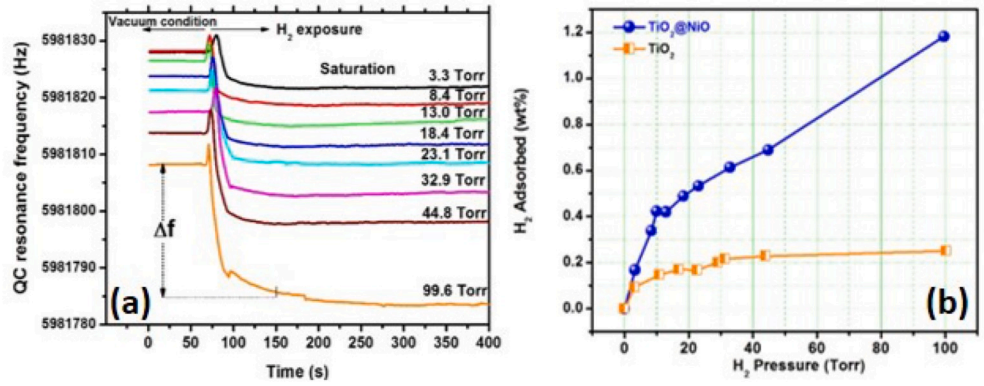

Fig. 5. Hydrogen adsorption isotherms of the pristine TiO_2 and NiO @ TiO_2. (a) Quartz-crystal (QC) resonance frequency as a function of time with different H_2 exposure pressure, (b) H_2 adsorption of pristine TiO_2 and NiO @ TiO_2 as a function of the H_2 exposure pressure.

of H_2 pressure which is ~5 times higher than that of as-obtained mesoporous TiO_2 (~0.25 wt%). This huge enhancement of hydrogen adsorption highlights the critical importance of the existence of Ti^{3+} in the heterostructure which is mainly induced by the creation of Ni^{3+} in the lattice. This enhancement is not due to physisorption because the mesoporous materials do not offer much hydrogen physisorption in very low pressure region. Furthermore, the NiO@TiO_2 has lower specific surface area than the pristine mesoporous TiO_2. In general, the unique creation of mixed-valence heterostructures impart efficient charge-transfer ability and facilitates excellent photocatalytic water splitting and hydrogen storage.

4. Conclusions

In summary, the surface defect induced formation of Ni^{3+} and Ti^{3+} near the interface of mesoporous heterostructure, NiO@TiO_2 with engineered bandgap were successfully explored by a facile route. The substantial amount of Ni^{3+} with near-unity occupancy of e_g orbital, and Ti^{3+} formation by the creation of more oxygen vacancies in the lattice promotes the rapid electron-hole separation processes, thus enhance the overall charge transfer efficiency, found to be 12 times higher hydrogen evolution (or 1200% enhancement) and ~5 times higher hydrogen adsorption (or 500% enhancement) than those of mesoporous TiO_2. This facile synthetic procedure for preparing defect-induced heterostructures opening up the solid pathways toward the excellent photocatalytic hydrogen production and storage.

Declaration of competing interest

The authors Kumar Raju, Saravanan Rajendran, Tuan K.A. Hoang, D. Durgalakshmi, Jiaqian Qin, D.E. Diaz-Droguett, F. Gracia, M. A. Gracia-Pinilla, declared that they have no known competing financial interests or personal relationships that could have appeared to influence the work reported in this paper.

The authors Kumar Raju, Saravanan Rajendran, Tuan K.A. Hoang, D. Durgalakshmi, Jiaqian Qin, D.E. Diaz-Droguett, F. Gracia, M. A. Gracia-Pinilla, declared that **there is no conflict of interest** regarding the publication of this article entitled on "**Photosynthesis of H_2 and its**

Storage on the Bandgap Engineered Mesoporous (Ni^{2+}/Ni^{3+})O @ TiO_2 Heterostructure".

CRediT authorship contribution statement

Kumar Raju: Writing - original draft. **Saravanan Rajendran:** Conceptualization, Methodology, Writing - review & editing. **Tuan K.A. Hoang:** Conceptualization, Methodology, Writing - review & editing. **D. Durgalakshmi:** Visualization, Investigation, Software, Validation. **Jiaqian Qin:** Visualization, Investigation, Software, Validation. **D.E. Diaz-Droguett:** Visualization, Investigation, Software, Validation. **F. Gracia:** Visualization, Investigation, Software, Validation. **M.A. Gracia-Pinilla:** Visualization, Investigation, Software, Validation.

Acknowledgement

The authors (S.R., F.G.) acknowledge the support of ANID through the project ANID/FONDAP/15110019. The author (S.R) acknowledge FONDECYT Government of Chile (Project No.: 11170414), for the support to carry out this project.

References

[1] B. Liu, L.M. Liu, X.F. Lang, H.Y. Wang, X.W. Lou, E.S. Aydil, Doping high-surface-area mesoporous TiO_2 microspheres with carbonate for visible light hydrogen production, Energy Environ. Sci. 7 (2014) 2592–2597, https://doi.org/10.1039/c4ee00472h.

[2] H. Bin Yang, J. Miao, S.F. Hung, F. Huo, H.M. Chen, B. Liu, Stable quantum dot photoelectrolysis cell for unassisted visible light solar water splitting, ACS Nano 8 (2014) 10403–10413, https://doi.org/10.1021/nn503751s.

[3] A. Fujishima, K. Honda, Electrochemical photolysis of water at a semiconductor electrode, Nature 238 (1972) 37–38, https://doi.org/10.1038/238038a0.

[4] J. Cai, J. Shen, X. Zhang, Y.H. Ng, J. Huang, W. Guo, C. Lin, Y. Lai, Hydrogen production: light-driven sustainable hydrogen production utilizing TiO_2 nanostructures: a review (small methods 1/2019), Small Method 3 (2019) 1800053, https://doi.org/10.1002/smtd.201870053.

[5] T. Hisatomi, K. Domen, Reaction systems for solar hydrogen production via water splitting with particulate semiconductor photocatalysts, Nat. Catal. 2 (2019) 387–399, https://doi.org/10.1038/s41929-019-0242-6.

[6] A.J. Cowan, J. Tang, W. Leng, J.R. Durrant, D.R. Klug, Water splitting by nanocrystalline TiO_2 in a complete photoelectrochemical cell exhibits efficiencies limited by charge recombination, J. Phys. Chem. C 114 (2010) 4208–4214, https://doi.org/10.1021/jp909993w.

[7] F.M. Pesci, G. Wang, D.R. Klug, Y. Li, A.J. Cowan, Efficient suppression of electron-hole recombination in oxygen-deficient hydrogen-treated TiO_2 nanowires for photoelectrochemical water splitting, J. Phys. Chem. C 117 (2013) 25837–25844, https://doi.org/10.1021/jp4099914.

[8] C. Dette, M.A. Pérez-Osorio, C.S. Kley, P. Punke, C.E. Patrick, P. Jacobson, F. Giustino, S.J. Jung, K. Kern, TiO_2 anatase with a bandgap in the visible region, Nano Lett. 14 (2014) 6533–6538, https://doi.org/10.1021/nl503131s.

[9] V. Kumaravel, S. Mathew, J. Bartlett, S.C. Pillai, Photocatalytic hydrogen production using metal doped TiO_2 : a review of recent advances, Appl. Catal. B Environ. 244 (2019) 1021–1064, https://doi.org/10.1016/j.apcatb.2018.11.080.

[10] X. Hu, X. Liu, J. Tian, Y. Li, H. Cui, Towards full-spectrum (UV, visible, and near-infrared) photocatalysis: achieving an all-solid-state Z-scheme between Ag_2O and TiO_2 using reduced graphene oxide as the electron mediator, Catal. Sci. Technol. 7 (2017) 4193–4205, https://doi.org/10.1039/c7cy01349c.

[11] M. Wang, Y. Hu, J. Han, R. Guo, H. Xiong, Y. Yin, TiO_2/NiO hybrid shells: P-n junction photocatalysts with enhanced activity under visible light, J. Mater. Chem. A. 3 (2015) 20727–20735, https://doi.org/10.1039/c5ta05839b.

[12] M.M. Khan, S.A. Ansari, D. Pradhan, M.O. Ansari, D.H. Han, J. Lee, M.H. Cho, Band gap engineered TiO_2 nanoparticles for visible light induced photoelectrochemical and photocatalytic studies, J. Mater. Chem. A. 2 (2014) 637–644, https://doi.org/10.1039/c3ta14052k.

[13] F. Feng, C. Li, J. Jian, X. Qiao, H. Wang, L. Jia, Boosting hematite photoelectrochemical water splitting by decoration of TiO_2 at the grain boundaries, Chem. Eng. J. 368 (2019) 959–967, https://doi.org/10.1016/j.cej.2019.03.005.

[14] Z. Jin, X. Zhang, Y. Li, S. Li, G. Lu, 5.1% Apparent quantum efficiency for stable hydrogen generation over eosin-sensitized CuO/TiO_2 photocatalyst under visible light irradiation, Catal. Commun. 8 (2007) 1267–1273, https://doi.org/10.1016/j.catcom.2006.11.019.

[15] H. Hou, M. Shang, F. Gao, L. Wang, Q. Liu, J. Zheng, Z. Yang, W. Yang, Highly efficient photocatalytic hydrogen evolution in ternary hybrid TiO2/CuO/Cu thoroughly mesoporous nanofibers, ACS Appl. Mater. Interfaces 8 (2016), https://doi.org/10.1021/acsami.6b06644, 20128–20137.

[16] X. Yu, J. Zhang, Z. Zhao, W. Guo, J. Qiu, X. Mou, A. Li, J.P. Claverie, H. Liu, NiO-TiO_2 p-n heterostructured nanocables bridged by zero-bandgap rGO for highly efficient photocatalytic water splitting, Nano. Energy 16 (2015) 207–217, https://doi.org/10.1016/j.nanoen.2015.06.028.

[17] J. Lin, J. Shen, R. Wang, J. Cui, W. Zhou, P. Hu, D. Liu, H. Liu, J. Wang, R. I. Boughton, Y. Yue, Nano-p-n junctions on surface-coarsened TiO_2 nanobelts with enhanced photocatalytic activity, J. Mater. Chem. 21 (2011) 5106–5113, https://doi.org/10.1039/c0jm04131a.

[18] E. Cui, G. Lu, Enhanced surface electron transfer by fabricating a core/shell Ni@NiO cluster on TiO_2 and its role on high efficient hydrogen generation under visible light irradiation, Int. J. Hydrogen Energy 39 (2014) 8959–8968, https://doi.org/10.1016/j.ijhydene.2014.03.258.

[19] J. Yan, S. Yang, Z. Xie, X. Li, W. Zhou, X. Zhang, Y. Fang, S. Zhang, F. Peng, Heterostructured CoO/3D-TiO_2 nanorod arrays for photoelectrochemical water splitting hydrogen production, J. Solid State Electrochem. 21 (2017) 455–461, https://doi.org/10.1007/s10008-016-3375-4.

[20] F.X. Xiao, J. Miao, H.B. Tao, S.F. Hung, H.Y. Wang, H. Bin Yang, J. Chen, R. Chen, B. Liu, One-dimensional hybrid nanostructures for heterogeneous photocatalysis and photoelectrocatalysis, Small 11 (2015) 2115–2131, https://doi.org/10.1002/smll.201402420.

[21] M. Ge, Q. Li, C. Cao, J. Huang, S. Li, S. Zhang, Z. Chen, K. Zhang, S.S. Al-Deyab, Y. Lai, One-dimensional TiO2 nanotube photocatalysts for solar water splitting, Adv. Sci. 4 (2017) 1–31, https://doi.org/10.1002/advs.201600152.

[22] L. Li, J. Yan, T. Wang, Z.J. Zhao, J. Zhang, J. Gong, N. Guan, Sub-10 nm rutile titanium dioxide nanoparticles for efficient visible-light-driven photocatalytic hydrogen production, Nat. Commun. 6 (2015) 1–10, https://doi.org/10.1038/ncomms6881.

[23] H. Sun, S. Zeng, Q. He, P. She, K. Xu, Z. Liu, Spiky TiO_2/Au nanorod plasmonic photocatalysts with enhanced visible-light photocatalytic activity, Dalton Trans. 46 (2017) 3887–3894, https://doi.org/10.1039/c7dt00345e.

[24] Q. Zhang, D.Q. Lima, I. Lee, F. Zaera, M. Chi, Y. Yin, A highly active titanium dioxide based visible-light photocatalyst with nonmetal doping and plasmonic metal decoration, Angew. Chem. Int. Ed. 50 (2011) 7088–7092, https://doi.org/10.1002/anie.201101969.

[25] J. Yu, L. Qi, M. Jaroniec, Hydrogen production by photocatalytic water splitting over Pt/TiO_2 nanosheets with exposed (001) facets, J. Phys. Chem. C 114 (2010) 13118–13125, https://doi.org/10.1021/jp104488b.

[26] A. Gallo, T. Montini, M. Marelli, A. Minguzzi, V. Gombac, R. Psaro, P. Fornasiero, V. Dal Santo, H2 production by renewables photoreforming on Pt-Au/TiO_2 catalysts activated by reduction, ChemSusChem 5 (2012) 1800–1811, https://doi.org/10.1002/cssc.201200085.

[27] H. Bahruji, M. Bowker, P.R. Davies, F. Pedrono, New insights into the mechanism of photocatalytic reforming on Pd/TiO_2, Appl. Catal. B Environ. 107 (2011) 205–209, https://doi.org/10.1016/j.apcatb.2011.07.015.

[28] A.T. Montoya, E.G. Gillan, Enhanced photocatalytic hydrogen evolution from transition-metal surface-modified TiO_2, ACS Omega 3 (2018) 2947–2955, https://doi.org/10.1021/acsomega.7b02021.

[29] M.T. Uddin, Y. Nicolas, C. Olivier, W. Jaegermann, N. Rockstroh, H. Junge, T. Toupance, Band alignment investigations of heterostructure NiO/TiO_2 nanomaterials used as efficient heterojunction earth-abundant metal oxide photocatalysts for hydrogen production, Phys. Chem. Chem. Phys. 19 (2017) 19279–19288, https://doi.org/10.1039/c7cp01300k.

[30] L. Liu, W. Yang, W. Sun, Q. Li, J.K. Shang, Creation of Cu_2O@TiO_2 composite photocatalysts with p - N heterojunctions formed on exposed Cu2O facets, their energy band alignment study, and their enhanced photocatalytic activity under illumination with visible light, ACS Appl. Mater. Interfaces 7 (2015) 1465–1476, https://doi.org/10.1021/am505861c.

[31] F. Kayaci, S. Vempati, C. Ozgit-Akgun, I. Donmez, N. Biyikli, T. Uyar, Selective isolation of the electron or hole in photocatalysis: ZnO-TiO_2 and TiO_2-ZnO core-shell structured heterojunction nanofibers via electrospinning and atomic layer deposition, Nanoscale 6 (2014) 5735–5745, https://doi.org/10.1039/c3nr06665g.

[32] S. ichiro Fujita, H. Kawamori, D. Honda, H. Yoshida, M. Arai, Photocatalytic hydrogen production from aqueous glycerol solution using NiO/TiO 2 catalysts: effects of preparation and reaction conditions, Appl. Catal. B Environ. 181 (2016) 818–824, https://doi.org/10.1016/j.apcatb.2015.08.048.

[33] L. Fan, J. Long, Q. Gu, H. Huang, H. Lin, X. Wang, Single-site nickel-grafted anatase TiO2 for hydrogen production: toward understanding the nature of visible-light photocatalysis, J. Catal. 320 (2014) 147–159, https://doi.org/10.1016/j.jcat.2014.09.020.

[34] J. Yu, Y. Hai, B. Cheng, Enhanced photocatalytic H_2-production activity of TiO_2 by $Ni(OH)_2$ cluster modification, J. Phys. Chem. C 115 (2011) 4953–4958, https://doi.org/10.1021/jp111562d.

[35] Q. Yang, M. Long, L. Tan, Y. Zhang, J. Ouyang, P. Liu, A. Tang, Helical TiO_2 nanotube Arrays modified by Cu-Cu_2O with ultrahigh sensitivity for the nonenzymatic electro-oxidation of glucose, ACS Appl. Mater. Interfaces 7 (2015) 12719–12730, https://doi.org/10.1021/acsami.5b03401.

[36] H.J. Gerritsen, E.S. Sabisky, Paramagnetic resonance of Ni^{2+} and Ni^{3+} in TiO_2, Phys Ical Rev 125 (1962) 1853. https://journals.aps.org/pr/pdf/10.1103/PhysRev.125.1853.

[37] Z. Xiu, M. Guo, T. Zhao, K. Pan, Z. Xing, Z. Li, W. Zhou, Recent advances in Ti 3 + self-doped nanostructured TiO_2 visible light photocatalysts for environmental and energy applications, Chem. Eng. J. (2019) 123011, https://doi.org/10.1016/j.cej.2019.123011.

[38] Y. Zhao, X. Jia, G. Chen, L. Shang, G.I.N. Waterhouse, L.Z. Wu, C.H. Tung, D. Ohare, T. Zhang, Ultrafine NiO nanosheets stabilized by TiO_2 from monolayer NiTi-LDH precursors: an active water oxidation electrocatalyst, J. Am. Chem. Soc. 138 (2016) 6517–6524, https://doi.org/10.1021/jacs.6b01606.

[39] Tuan K.A. Hoang, David M. Antonelli, Exploiting the Kubas interaction in the design of hydrogen storage materials, Adv. Mater. 21 (2000) 1787–1800, https://doi.org/10.1002/adma.200802832.

[40] A. Hamaed, Tuan K.A. Hoang, M. Trudeau, David M. Antonelli, Optimization of hydrogen storage capacity in silica-supported low valent Ti systems exploiting Kubas binding of hydrogen, J. Organomet. Chem. 694 (2009) 2793–2800, https://doi.org/10.1016/j.jorganchem.2009.02.034.

[41] Tuan K.A. Hoang, L. Morris, D. Reed, D. Book, Michel L. Trudeau, David M. Antonelli, Observation of TiH_5 and TiH_7 in Bulk-Phase TiH_3 gels for Kubas-type hydrogen storage, Chem. Mater. 25 (2013) 4765–4771, https://doi.org/10.1021/cm402853k.

[42] Tuan K.A. Hoang, L. Morris, J. Sun, Michel L. Trudeau, David M. Antonelli, Titanium hydrazide gels for Kubas-type hydrogen storage, J. Mater. Chem. A. 1 (2013) 1947–1951, https://doi.org/10.1039/C2TA00795A.

[43] S. Rajendran, D. Manoj, K. Raju, D.D. Dionysiou, M. Naushad, F. Gracia, L. Cornejo, M.A. Gracia-Pinilla, T. Ahamad, Influence of mesoporous defect induced mixed-valent NiO (Ni^{2+}/Ni^{3+})-TiO_2 nanocomposite for non-enzymatic glucose biosensors, Sensor. Actuator. B Chem. 264 (2018) 27–37, https://doi.org/10.1016/j.snb.2018.02.165.

[44] S. Rajendran, KA Hoang Tuan, R. Boukherroub, DE Diaz-Droguett, F. Gracia, M. A. Gracia-Pinilla, A. Akbari-Fakhrabadi, Vinod Kumar Gupta, Hydrogen adsorption properties of Ag decorated TiO_2 nanomaterials, Int. J. Hydrogen Energy 43 (2018) 2861–2868, https://doi.org/10.1016/j.ijhydene.2017.12.080.

[45] V.M. Mecea, From quartz crystal microbalance to fundamental principles of mass measurements, Anal. Lett. 38 (2005) 753–767, https://doi.org/10.1081/AL-200056171.

[46] E. Mosquera, D.E. Diaz-Droguett, N. Carvajal, M. Roble, M. Morel, R. Espinoza, Characterization and hydrogen storage in multi-walled carbon nanotubes grown by aerosol-assisted CVD method, Diam. Relat. Mater. 43 (2014) 66–71, https://doi.org/10.1016/j.diamond.2014.01.016.

[47] W. Hong, Y. Zhou, C. Lv, Z. Han, G. Chen, NiO quantum dot modified TiO2 toward robust hydrogen production performance, ACS Sustain. Chem. Eng. 6 (2018) 889–896, https://doi.org/10.1021/acssuschemeng.7b03250.

[48] G.J. Kubas, Fundamentals of H 2 binding and reactivity on transition metals underlying hydrogenase function and H_2 production and storage, Chem. Rev. 107 (2007) 4152–4205, https://doi.org/10.1021/cr050197j.